Free vibration analysis of sandwich FGM shells using isogeometric B-spline finite strip method

Mohammad Amin Shahmohammadi[a], Mojtaba Azhari* and Mohammad Mehdi Saadatpour[b]

Department of Civil Engineering, Isfahan University of Technology, Isfahan, Iran, P.O. Box 84156-83111

Abstract. This paper presents a free vibration analysis of shell panels made of functionally graded material (FGM) in the form of the ordinary and sandwich FGM and laminated shells using the isogeometric B3-spline finite strip method (IG-SFSM). B3-spline and Lagrangian interpolation are employed along the longitudinal and transverse directions respectively in this type of finite strip. The introduced finite strip formulation is based on the degenerated shell method, which provides variable thickness, arbitrary geometries, and analysis of thin or thick shells. Validity of the obtained natural frequencies by IG-SFSM is checked by comparison with results extracted from references for similar cases in different examples. These examples incorporate several geometries, materials, boundary conditions, and continuous thickness variation. A comparison of these two kinds of results and their proximity showed that the introduced IG-SFSM is a reliable tool which can be used in analysis of shells with the aforementioned properties.

Keywords: isogeometric B3-spline finite strip; natural frequencies; sandwich FGM and laminated shell panels; degenerated shell; variable thickness; arbitrary geometries; free vibration

1. Introduction

Several structural elements may be used to solve mechanical problems. Shell element is one of the most important of these and is widely used in aerospace, and civil and mechanical engineering. Due to difficulties and restrictions in analysis of shell structures using traditional and classical methods, the most appropriate approach is to employ numerical methods. The most prevalent method herein is finite element (FE), based on different theories like classical, first and higher order theories (CLT, FSDT, HSDT), or the degenerated shell method. Considerable research has been done on this subject (Ventsel and Krauthammer 2001). Elements introduced by researchers Chieslar and Ghali (1987) and Dvorkin and Bathe (1984) are continuum finite shell elements based on the degenerated shell method for general analysis. Review of existing literature related to shell structures demonstrates that developed elements based on the degenerated shell method have been favored more by researchers. Rezaiee-Pajand and Arabi (2016) and Jabareen and Mtanes (2018) developed curved triangular shell elements for nonlinear analysis of laminated shells and Cosserat point shell elements respectively based on the degenerated solid shell approach. Static and free vibration behavior of orthotropic elliptic paraboloid shells investigated by Darilmaz (2017)

by means of the element developed by combining a hybrid plane stress element and a hybrid plate element.

The major inefficiency corresponding to FEM is the large number of DOFs required for some problems, which makes utilizing a huge computer storage and solution time. In order to overcome this inefficiency, alternative methods are used in many researches, such as the finite strip method. The corresponding results for several cases, indicate that the finite strip method is more efficient than the general finite element method. This efficiency is related to the reduction of DOFs needed to obtain accurate results. Furthermore, the buckling of plates using the ordinary finite strip method has been performed by Benson and Hinton (1976). And-Van Erp and Menken (1990) for linear elastic and Kwon and Hancock (1991) for nonlinear elastic material: this allowed stability analysis of thin-walled section beams by the spline finite strip method (SFSM). Further research related to analysis of thin-walled structures by the finite strip method is about the structural analysis of shell structures using this specific method (Fan and Cheung 1983, Li *et al.* 1990, Hu 1997, Wang and Dawe 1999). Au and Cheung (1996) carried out bending, free vibration and stability analysis of isotropic shells using the isoparametric spline finite strip method (ISFSM). In order to satisfy the different boundary conditions (BCs), they used additional points out of the structure's domain and undertook extrapolation of the geometry. Sheikh (2004) used SFSM in order to analyze thick composite structures. Eccher *et al.* (2008) developed a specific isoparametric spline finite strip (ISFSM) to analyze perforated thin-walled structures based on the first-order shear deformation theory. Foroughi and Azhari (2014) investigated mechanical buckling and free vibration of thick functionally graded plates resting on an elastic foundation

---

*Corresponding author, Professor
 E-mail: mojtaba@cc.iut.ac.ir
[a]Ph.D. Student
[b]Ph.D.

using the higher-order B-spline finite strip method. Naghsh *et al.* (2015) implemented free vibration analysis of stringer stiffened general shells of revolution using the meridional finite strip method. Beside the advantages and efficiencies of the older FSM versions, they have two major shortcomings. Since FSM is basically developed for analysis of the plates or shallow shells with simple geometries (Au and Cheung 1996, Benson and Hinton 1976), it suffers from the weakness of applying various boundary conditions and mapping procedure to analyze the shells with complicated geometries.

The other efficient numerical method is isogeometric analysis (IGA), which is based on B-spline and NURBS interpolation in all of the curvilinear directions. Contrary to FEM and older versions of FSM, which approximate the geometry, IGA represents the exact one. It leads to provide higher-order accuracy comparing to FEM by utilizing the same number of DOFs. Employing IGA provides the higher-order continuity between the elements, while most of the FEM used in shell analysis, only provide C^0-continuity. However, isogeometric analysis has some shortcomings in use of the method in many problems which can be solved by means of FEM with no difficulties. By employing B-spline interpolation in 2D and 3D IGA and constructing rectangular grid of control points, the purely local refinement is so complicated and requires additional unwanted knots in the B-spline parameter space (Kim *et al.* 2010, Nguyen *et al.* 2015). The other shortcoming of IGA is the weakness of applying the Dirichlet BCs at control points of rectangular control-grid, which are not located at the boundaries. It means that some especial treatment techniques such as Lagrange multiplier method or defining the penalty functions, are required for some especial cases. Contrarily, by employing FEM, it is possible to impose Dirichlet BCs at boundary nodes, directly (Rypl and Patzák, 2012).

In order to carry out free vibration analysis, there are some other methods in literature, which are based on the various theories to solve especial problems. Tornabene and Viola (2009) carried out free vibration analysis of functionally graded panels and shells of revolution by means of the GDQ method. Similar work for vibration analysis of laminated and sandwich FGM plates and shells of varying thickness has been done by Bacciocchi *et al.* (2015) and Tornabene *et al.* (2017) respectively. Younsi *et al.* (2018) carried out bending and free vibration analysis of FGM plates by means of hyperbolic shape functions based on quasi-3D and 2D shear deformation theories. Bourada *et al.* (2015) considered the effects of thickness stretching on bending and vibration of functionally graded beams. Free vibration of functionally graded nanoscale plates, beams and shells are investigated in (Bounouara *et al.* 2016, Zemri *et al.* 2015, Karami *et al.* 2018). Bourada *et al.* (2019) investigated the dynamic behavior of porous functionally graded beams by using a sinusoidal shear deformation theory. Stability, bending and vibration analyses of the sandwich FGM plates and shells, are important portions of thin-walled structures analysis. In this regard, Abdelaziz *et al.* (2017) and Belabed *et al.* (2018) performed buckling, bending and free vibration analyses of the sandwich FGM

plates based on hyperbolic shear deformation theory. Menasria *et al.* (2017) and El-Haina *et al.* (2017) investigated thermal stability of FGM sandwich plates.

Various structural problems have been solved using interpolation by B-spline functions (Dawe and Wang 1992, Van Erp *et al.* 1994, Uhm and Youn 2009, Fan and Luah 1990, Vu-Bac *et al.* 2018). Some other related problems have been solved using analytical solutions (Javad *et al.* 2016, Shahmohamadi and Kabir 2017, Pang *et al.* 2018, Zine *et al.* 2018).

By considering the aforementioned studies especially researches which are related to analysis of thin-walled structures by means of the finite strip method, it is clear that there are some deficiencies in this corpus of work. Some studies are limited to special geometry or material and some additional knots out of the structure's domain are necessarily needed to satisfy the different boundary conditions using SFSM. This causes some difficulties, because these additional knots are not determinate and to find them the points inside the domain of the structure need extrapolation (Au and Cheung 1996, Eccher *et al.* 2008, Fan and Cheung 1983).

However, by considering the efficiencies and drawbacks of IGA and FEM, it seems that a novel method can be developed with multipurpose targets by applying the combination of FEM and IGA in free vibration analysis of the sandwich FGM shells. In the current work, a novel version of finite strip, namely, the isogeometric spline finite strip method (IG-SFSM) is developed, which applies FEM and IGA based on B_3-spline basis functions in the transversal and longitudinal directions, respectively. The method provides the continuity of the finite strip shell elements in the longitudinal direction and reduces the IGA drawbacks by employing the FEM in the transversal direction. In order to simplicity of applying various boundary conditions after formation of the stiffness matrix, the B_3-spline basis functions are developed in way that Kronecker delta properties at the boundaries is provided (Piegl and Tiller 1997).

In the present study, integration in the thickness direction of the introduced IG-SFSM was performed during the formation of the stiffness matrix. This situation allows us to assume the properties of various materials (isotropic, laminated or sandwich FGM) and the variable thickness by a unit formulation. By means of the presented formulation, the function of variation thickness field and material properties were determined. Moreover, numerical integration along the three directions was based on the Gauss quadrature method.

The layout of the paper is as follows. In Section 2 the manner of the B-spline interpolation using data-points is presented. Section 3 denotes the formulation of the introduced IG-SFSM incorporating the manner of mapping, governing kinematic equations, formation of stiffness and mass matrices, and definition of functionally graded material (FGM). In Section 4, to show the efficiency of the introduced finite strip method, different examples are provided to obtain the natural frequency parameters. Finally, in Section 5, conclusions of this paper are summarized.
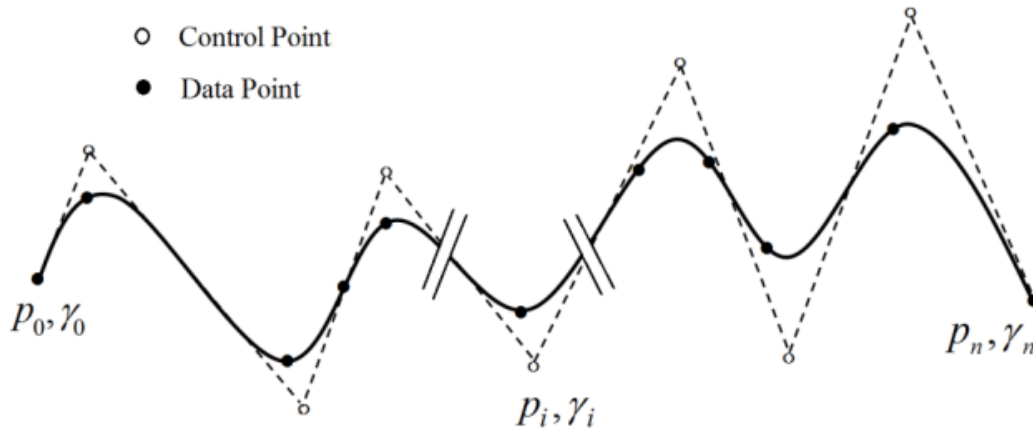
Fig. 1 Schematic view of the B-spline curve C with data and control points

2. Interpolation using basis B-spline functions

The most important portion of numerical methods to solve structural problems especially FEM and FSM is the manner of interpolation. There are various methods for interpolation like Lagrange and spline interpolation. Each of these methods has some advantages and disadvantages. In the present paper Lagrange and spline methods have been use for interpolation in transverse and longitudinal directions respectively. The most important reason for using spline interpolation along the longitudinal direction of strips is the special characteristics of spline functions. Interpolation in the longitudinal direction should be implemented by several points as compared to the transverse direction of a strip. Spline interpolation avoids oscillation at the edges of the intervals by interpolating through high degree polynomials: this method is distinct from the number of data points using polynomials with low degrees (Piegl and Tiller 1997). In the present paper, displacement field and components of the global coordinate system are interpolated using B_3-spline basis functions.

Interpolation of the curve C with some data points using B-spline basis functions was according to Eq. (1)

$$C : f(\eta) = \sum_{i=0}^{n} \phi_{i,p}(\eta)\gamma_i \qquad (1)$$

where γ_i denotes ith control point demonstrated in Fig. 1, and $\phi_{i,p}$ illustrates the ith basis B-spline function and p denotes order of basis B-spline functions. Fig. 1 shows a schematic view of the B-spline curve C with data and control points.

The ith normalized basis B-spline function ($\phi_{i,p}$) demonstrated in Eq. (1) is defined by a recursive equation, as shown in Eq. (2)

$$\phi_{i,0} = \begin{cases} 1 & \eta_i \le \eta \le \eta_{i+1} \\ 0 & otherwise \end{cases}$$

$$t = \left\langle \eta_0 \quad \eta_1 \quad \cdots \quad \eta_{n+p+1} \right\rangle \qquad (2)$$

$$\phi_{i,p} = \frac{\eta - \eta_i}{\eta_{i+p} - \eta_i}\phi_{i,p-1} + \frac{\eta_{i+p+1} - \eta}{\eta_{i+p+1} - \eta_{i+1}}\phi_{i+1,p-1}$$

B-spline basis functions are defined by the knot vector (t) presented in Eq. (2). Note that the derivatives of the B-spline basis functions of order p can be written in the form of a recursive equation by two B-splines of a lower order. This is presented in Eq. (3) (Piegl and Tiller 1997)

$$\phi_{i,p}^{(j)} = p\left(\frac{\phi_{i,p-1}^{(j-1)}}{\eta_{i+p} - \eta_i} - \frac{\phi_{i+1,p-1}^{(j-1)}}{\eta_{i+p+1} - \eta_{i+1}}\right) \qquad (3)$$

Solving mechanical problems using B-spline interpolation has a special characteristic which satisfies the general boundary conditions. If knot values at the boundaries repeat with multiplicity equal to $p+1$, as mentioned in Eq. (4), then the B-spline basis functions so obtained provide the Kronecker delta properties at the boundaries. By means of this property, it is possible to satisfy the arbitrary boundary condition after formation of stiffness, mass matrices and force vector.

$$t = \left\langle \underbrace{\eta_0, ..., \eta_0}_{p+1}, \eta_1, ..., \eta_{ns-1}, \underbrace{\eta_{ns}, ..., \eta_{ns}}_{p+1} \right\rangle \qquad (4)$$

Note that B-spline interpolation is possible only when the number of control points is equal to data points. To set this condition, the value of ns presented in Eq. (4) should be equal to $n - p + 1$. The value of n denotes the number of intervals. So, the value of $n+1$ represents the number of control or data points. For example, let us assume that there are 9 control and data points and that the order of B-
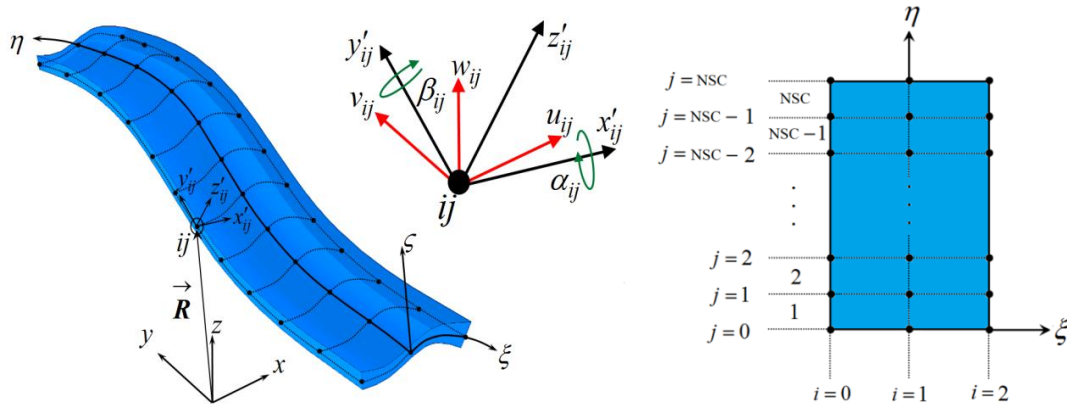
Fig. 2 An example of general finite strip in global and local curvilinear coordinates with arbitrary shape, variable thickness, and assumed DOFs

spline basis functions is 3. For this situation the values of n and ns should be 8 and 6 respectively. In Eq. (1), all of the control points (γ_i) are related to the geometry of the curve and can be calculated using the existing data points (p_i) on the curve. Substituting data points in Eq. (1) yields the linear system of equations with $n+1$ equations and $n+1$ unknowns: the values of control points can be calculated in this manner (Piegl and Tiller 1997).

3. Isogeometric B3-spline finite strip method

In this section, a new version of finite strip is developed: it is called the isogeometric B3-spline finite strip method (IG-SFSM). Within this type of FSM, interpolation of components of the global coordinate system and the displacement field in longitudinal and transverse directions can be performed by the B3-spline and Lagrangian functions respectively. IG-SFSM provides the ability to model shells with complex geometries and boundary conditions.

3.1 Mapping

Consider a general shape finite strip element with variable thickness as shown in Fig. 2. The relevant transverse quadratic Lagrangian shape functions are given in Eq. (5)

$$L_0(\xi) = \frac{1}{2}\xi(\xi - 1), \quad L_1(\xi) = -(\xi + 1)(\xi - 1)$$
$$L_2(\xi) = \frac{1}{2}\xi(\xi + 1) \tag{5}$$

where $L_i(\xi)$ represents the Lagrangian quadratic shape function of the ith nodal line in local transverse curvilinear direction (ξ), (Fig. 2). The functions used for the local longitudinal curvilinear direction (η) and their properties are demonstrated in Eqs. (2)-(4). The general form of the

global coordinate system x, y, z in terms of the components of the local curvilinear coordinate system ξ, η by the B3-spline and the Lagrangian shape functions can be expressed as follows

$$\begin{Bmatrix} x(\xi,\eta) \\ y(\xi,\eta) \\ z(\xi,\eta) \end{Bmatrix} = \sum_{i=0}^{2}\sum_{j=0}^{NSC} N_{ij}(\xi,\eta)\left\{ \begin{Bmatrix} \gamma_{ij}^x \\ \gamma_{ij}^y \\ \gamma_{ij}^z \end{Bmatrix} + \frac{\zeta h_{ij}}{2}\begin{Bmatrix} (l_{3ij})_\gamma \\ (m_{3ij})_\gamma \\ (n_{3ij})_\gamma \end{Bmatrix} \right\}$$
$$\equiv \boldsymbol{x}(\xi,\eta) = \boldsymbol{n}\left(\hat{\boldsymbol{\gamma}}^x + \frac{\zeta}{2}(\boldsymbol{V}_3)_\gamma \right) \tag{6}$$
$$* N_{ij}(\xi,\eta) = L_i(\xi)\phi_{j,3}(\eta)$$

Coefficients $\gamma_{ij}^x, \gamma_{ij}^y, \gamma_{ij}^z$ are control points related to the global coordinates of the node ij (x_{ij}, y_{ij}, z_{ij}): they are located at ith nodal line and jth row of nodes, and $(l_{3ij})_\gamma, (m_{3ij})_\gamma, (n_{3ij})_\gamma$ are direction cosines related to these control points. All the unknown coefficients related to the control points are geometry dependent of the shell. Using data points on the mid-surface of the shell and substituting into Eq. (6), a linear system of equations is formed with $9(NSC + 1)$ equations and unknowns. This process is mentioned in Eq. (7)

$$\begin{Bmatrix} x_{ij} \\ y_{ij} \\ z_{ij} \end{Bmatrix} = \begin{Bmatrix} x(\xi_{ij},\eta_{ij}) \\ y(\xi_{ij},\eta_{ij}) \\ z(\xi_{ij},\eta_{ij}) \end{Bmatrix} = \sum_{i=0}^{2}\sum_{j=0}^{NSC} N_{ij}(\xi_{ij},\eta_{ij})\begin{Bmatrix} \gamma_{ij}^x \\ \gamma_{ij}^y \\ \gamma_{ij}^z \end{Bmatrix} \tag{7}$$
$$\Rightarrow \hat{\boldsymbol{x}} = \boldsymbol{\Phi}\hat{\boldsymbol{\gamma}}^x \Rightarrow \hat{\boldsymbol{\gamma}}^x = \boldsymbol{\Phi}^{-1}\hat{\boldsymbol{x}}$$

Shape function of the shell strip element can be modified for usage of data points by substituting Eq. (7) into Eq. (6) for the case $\zeta = 0$

$$\zeta = 0: \quad \boldsymbol{x}(\xi,\eta) = \boldsymbol{n}\hat{\boldsymbol{\gamma}}^{\boldsymbol{x}} = \boldsymbol{n}\boldsymbol{\Phi}^{-1}\hat{\boldsymbol{x}} = \bar{\boldsymbol{n}}\hat{\boldsymbol{x}} \quad (8)$$

where

$$\boldsymbol{n} = \begin{bmatrix} & \vdots & N_{ij} & 0 & 0 & \vdots & \\ \cdots & \vdots & 0 & N_{ij} & 0 & \vdots & \cdots \\ & \vdots & 0 & 0 & N_{ij} & \vdots & \end{bmatrix}$$

$$\bar{\boldsymbol{n}} = \begin{bmatrix} & \vdots & \bar{N}_{ij} & 0 & 0 & \vdots & \\ \cdots & \vdots & 0 & \bar{N}_{ij} & 0 & \vdots & \cdots \\ & \vdots & 0 & 0 & \bar{N}_{ij} & \vdots & \end{bmatrix} \quad (9)$$

Using a similar interpretation, it is possible to use data points instead of control points for components of the global coordinate system and displacement by using the modified shape function $(\bar{\boldsymbol{n}})$ instead of the initial one $(\boldsymbol{n})$.

$$\begin{Bmatrix} x(\xi,\eta) \\ y(\xi,\eta) \\ z(\xi,\eta) \end{Bmatrix} = \sum_{i=0}^{2}\sum_{j=0}^{NSC} N_{ij}(\xi,\eta)\left\{ \begin{Bmatrix} x_{ij} \\ y_{ij} \\ z_{ij} \end{Bmatrix} + \frac{\zeta\, h_{ij}}{2}\begin{Bmatrix} l_{3ij} \\ m_{3ij} \\ n_{3ij} \end{Bmatrix} \right\} \quad (10)$$

$$\equiv \boldsymbol{x}(\xi,\eta) = \bar{\boldsymbol{n}}\left(\hat{\boldsymbol{x}} + \frac{\zeta}{2}\boldsymbol{V}_3\right)$$

Using Eq. (10), the Jacobian matrix is calculable as

$$\boldsymbol{J} = \begin{bmatrix} \frac{\partial x}{\partial \xi} & \frac{\partial y}{\partial \xi} & \frac{\partial z}{\partial \xi} \\ \frac{\partial x}{\partial \eta} & \frac{\partial y}{\partial \eta} & \frac{\partial z}{\partial \eta} \\ \frac{\partial x}{\partial \zeta} & \frac{\partial y}{\partial \zeta} & \frac{\partial z}{\partial \zeta} \end{bmatrix} = \begin{bmatrix} J_{11} & J_{12} & J_{13} \\ J_{21} & J_{22} & J_{23} \\ J_{31} & J_{32} & J_{33} \end{bmatrix}, \quad \boldsymbol{J}^{-1} = \boldsymbol{J}^{*} \quad (11)$$

3.2 Displacement field and kinematic equations

Displacement field of a finite strip based on the degenerated shell method is expressed in Eq. (12), developed using concepts in Eqs. (1)-(6) and the DOFs depicted in Fig. 2. Displacement field demonstrated in Eq. (12) has been written based on displacement fields expressed in (Dvorkin and Bathe 1984, Chieslar and Ghali 1987, Au and Cheung 1996, Rezaiee-Pajand and Arabi 2016, Jabareen and Mtanes 2018) for a finite shell element.

$$\begin{Bmatrix} u \\ v \\ w \end{Bmatrix} = \sum_{i=0}^{2}\sum_{j=0}^{NSC} N_{ij}\begin{bmatrix} 1 & 0 & 0 & -\zeta\frac{h_{ij}}{2}(l_{2ij})_\gamma & \zeta\frac{h_{ij}}{2}(l_{1ij})_\gamma \\ 0 & 1 & 0 & -\zeta\frac{h_{ij}}{2}(m_{2ij})_\gamma & \zeta\frac{h_{ij}}{2}(m_{1ij})_\gamma \\ 0 & 0 & 1 & -\zeta\frac{h_{ij}}{2}(n_{2ij})_\gamma & \zeta\frac{h_{ij}}{2}(n_{1ij})_\gamma \end{bmatrix}\begin{Bmatrix} \gamma_{ij}^u \\ \gamma_{ij}^v \\ \gamma_{ij}^w \\ \gamma_{ij}^\alpha \\ \gamma_{ij}^\beta \end{Bmatrix} \quad (12)$$

$$\equiv \boldsymbol{u} = \sum_{i=0}^{2}\sum_{j=0}^{NSC} \boldsymbol{N}^{ij}\hat{\boldsymbol{\gamma}}_{ij}^u$$

Where coefficients $\gamma_{ij}^u, \gamma_{ij}^v, \gamma_{ij}^w, \gamma_{ij}^\alpha, \gamma_{ij}^\beta$ are the control points related to the nodal DOFs located in the ith nodal line and the jth row of nodes $(u_{ij}, v_{ij}, w_{ij}, \alpha_{ij}, \beta_{ij})$. Note

that u_{ij}, v_{ij}, w_{ij} are nodal translational DOFs in the direction of the components of the global coordinate system (x, y, z) and that α_{ij}, β_{ij} are nodal rotational DOFs around the components of the local coordinate system $(x'(\text{or } \xi), y'(\text{or } \eta))$ respectively. Using the concept denoted in Eq. (7), it is possible to rewrite Eq. (12) based on the data points of the nodal DOFs as illustrated in Eq. (13)

$$\begin{Bmatrix} u \\ v \\ w \end{Bmatrix} = \sum_{i=0}^{2}\sum_{j=0}^{NSC} \bar{N}_{ij}\begin{bmatrix} 1 & 0 & 0 & -\zeta\frac{h_{ij}}{2}l_{2ij} & \zeta\frac{h_{ij}}{2}l_{1ij} \\ 0 & 1 & 0 & -\zeta\frac{h_{ij}}{2}m_{2ij} & \zeta\frac{h_{ij}}{2}m_{1ij} \\ 0 & 0 & 1 & -\zeta\frac{h_{ij}}{2}n_{2ij} & \zeta\frac{h_{ij}}{2}n_{1ij} \end{bmatrix}\begin{Bmatrix} u_{ij} \\ v_{ij} \\ w_{ij} \\ \alpha_{ij} \\ \beta_{ij} \end{Bmatrix} \quad (13)$$

$$\equiv \boldsymbol{u} = \sum_{i=0}^{2}\sum_{j=0}^{NSC} \bar{\boldsymbol{N}}^{ij}\hat{\boldsymbol{u}}_{ij}$$

Now we can introduce kinematic equations based on 3D elasticity through Eq. (14)

$$\varepsilon_x = \frac{\partial u}{\partial x} \qquad \varepsilon_x = \frac{\partial v}{\partial y} \qquad \varepsilon_x = \frac{\partial w}{\partial z}$$

$$\gamma_{xy} = \frac{\partial u}{\partial y} + \frac{\partial v}{\partial x} \qquad \gamma_{yz} = \frac{\partial v}{\partial z} + \frac{\partial w}{\partial y} \qquad (14)$$

$$\gamma_{xz} = \frac{\partial u}{\partial z} + \frac{\partial w}{\partial x}$$

Substituting Eq. (13) into Eq. (14) yields

$$\begin{Bmatrix} u \\ v \\ w \end{Bmatrix} = \sum_{i=0}^{2}\sum_{j=0}^{NSC} \begin{bmatrix} a_{ij} & 0 & 0 \\ 0 & b_{ij} & 0 \\ 0 & 0 & c_{ij} \\ b_{ij} & a_{ij} & 0 \\ 0 & c_{ij} & b_{ij} \\ c_{ij} & 0 & a_{ij} \end{bmatrix}$$

$$\cdots \begin{bmatrix} -d_{ij}l_{2ij} & d_{ij}l_{1ij} \\ -e_{ij}m_{2ij} & e_{ij}m_{1ij} \\ -f_{ij}n_{2ij} & f_{ij}n_{1ij} \\ -e_{ij}l_{2ij}-d_{ij}m_{2ij} & e_{ij}l_{1ij}+d_{ij}m_{1ij} \\ -f_{ij}m_{2ij}-e_{ij}n_{2ij} & f_{ij}m_{1ij}+e_{ij}n_{1ij} \\ -d_{ij}n_{2ij}-f_{ij}l_{2ij} & d_{ij}n_{1ij}+f_{ij}l_{1ij} \end{bmatrix}\begin{Bmatrix} u_{ij} \\ v_{ij} \\ w_{ij} \\ \alpha_{ij} \\ \beta_{ij} \end{Bmatrix} \quad (15)$$

$$\equiv \hat{\boldsymbol{\varepsilon}} = \sum_{i=0}^{2}\sum_{j=0}^{NSC} \boldsymbol{B}^{ij}\hat{\boldsymbol{u}}_{ij} = \boldsymbol{B}\hat{\boldsymbol{u}}$$

where

$$\begin{Bmatrix} a_{ij} \\ b_{ij} \\ c_{ij} \end{Bmatrix} = \begin{bmatrix} J_{11}^* & J_{12}^* \\ J_{21}^* & J_{22}^* \\ J_{31}^* & J_{32}^* \end{bmatrix} \begin{Bmatrix} \overline{N}_{ij,\xi} \\ \overline{N}_{ij,\eta} \end{Bmatrix}$$

$$\begin{Bmatrix} d_{ij} \\ e_{ij} \\ g_{ij} \end{Bmatrix} = \frac{h_{ij}}{2} \left(\zeta \begin{Bmatrix} a_{ij} \\ b_{ij} \\ c_{ij} \end{Bmatrix} + \overline{N}_{ij} \begin{Bmatrix} J_{13}^* \\ J_{23}^* \\ J_{33}^* \end{Bmatrix} \right)$$

(16)

3.3 Free vibration analysis

Stiffness matrix can be obtained using virtual work method expressed in Eq. (17)

$$\delta U = \int_V \delta\hat{\boldsymbol{\varepsilon}}^T \hat{\boldsymbol{\sigma}} dV = \int_V \delta\hat{\boldsymbol{\varepsilon}}^T \boldsymbol{D}\hat{\boldsymbol{\varepsilon}} dV = \delta\hat{\boldsymbol{u}}^T \left(\int_V \boldsymbol{B}^T \boldsymbol{D}\boldsymbol{B} dV \right) \hat{\boldsymbol{u}}$$

$$= \delta\hat{\boldsymbol{u}}^T \left(\int_{-1}^1 \int_{-1}^{ns} \int_{-1}^1 \boldsymbol{B}^T \boldsymbol{D}\boldsymbol{B} \det(\boldsymbol{J}) d\xi d\eta d\zeta \right) \hat{\boldsymbol{u}} =$$

$$= \delta\hat{\boldsymbol{u}}^T \left(\boldsymbol{K}_{strip} \right) \hat{\boldsymbol{u}}$$

(17)

where δU is variation of strain energy and

$$\hat{\boldsymbol{\sigma}} = \left\langle \sigma_x \quad \sigma_y \quad \sigma_z \quad \tau_{xy} \quad \tau_{yz} \quad \tau_{xz} \right\rangle^T$$

$$\hat{\boldsymbol{\varepsilon}} = \left\langle \varepsilon_x \quad \varepsilon_y \quad \varepsilon_z \quad \gamma_{xy} \quad \gamma_{yz} \quad \gamma_{xz} \right\rangle^T$$

$$\boldsymbol{D}(\xi,\eta,\zeta) = \boldsymbol{T}^T(\xi,\eta)\overline{\boldsymbol{D}}(\zeta)\boldsymbol{T}(\xi,\eta)$$

(18)

Transformation matrix, $\boldsymbol{T}$ and elasticity coefficients matrix, $\overline{\boldsymbol{D}}$ can be calculated using Eq. (19)

$$\overline{\boldsymbol{D}}(\zeta) = \frac{E(\zeta)}{(1-\nu^2)} \begin{bmatrix} 1 & \nu(\zeta) & 0 & 0 & 0 & 0 \\ \nu(\zeta) & 1 & 0 & 0 & 0 & 0 \\ 0 & 0 & 1 & 0 & 0 & 0 \\ 0 & 0 & 0 & \frac{1-\nu(\zeta)}{2} & 0 & 0 \\ 0 & 0 & 0 & 0 & \frac{1-\nu(\zeta)}{2\alpha} & 0 \\ 0 & 0 & 0 & 0 & 0 & \frac{1-\nu(\zeta)}{2\alpha} \end{bmatrix}$$

$$\boldsymbol{T} = \begin{bmatrix} l_1^2 & m_1^2 & n_1^2 & l_1 m_1 \\ l_2^2 & m_2^2 & n_2^2 & l_2 m_2 \\ l_3^2 & m_3^2 & n_3^2 & l_3 m_3 \\ 2l_1 l_2 & 2m_1 m_2 & 2n_1 n_2 & l_1 m_2 + l_2 m_1 \\ 2l_3 l_2 & 2m_3 m_2 & 2n_3 n_2 & l_3 m_2 + l_2 m_3 \\ 2l_3 l_1 & 2m_3 m_1 & 2n_3 n_1 & l_3 m_1 + l_1 m_3 \end{bmatrix} \dots$$

(19)

$$\dots \begin{bmatrix} n_1 l_1 & m_1 n_1 \\ n_2 l_2 & m_2 n_2 \\ n_3 l_3 & m_3 n_3 \\ n_1 l_2 + n_2 l_1 & m_1 n_2 + m_2 n_1 \\ n_3 l_2 + n_2 l_3 & m_3 n_2 + m_2 n_3 \\ n_3 l_1 + n_1 l_3 & m_3 n_1 + m_1 n_3 \end{bmatrix}$$

$$\alpha = 1.2$$

In Eq. (19), parameters (l_i, m_i, n_i, where $i = 1, 2, 3$) are direction cosines of unit vectors at each integration point. $E(\zeta)$ is the elasticity module of the shell. A similar approach can be employed to obtain the mass matrix of a strip using virtual work

$$\delta V = \int_V \delta\dot{\boldsymbol{u}}^T \rho\ddot{\boldsymbol{u}} dV = \delta\hat{\dot{\boldsymbol{u}}}^T \left(\int_V \overline{\boldsymbol{N}}^T \rho\overline{\boldsymbol{N}} dV \right) \hat{\ddot{\boldsymbol{u}}} =$$

$$= \delta\hat{\dot{\boldsymbol{u}}}^T \left(\boldsymbol{M}_{strip} \right) \hat{\ddot{\boldsymbol{u}}}$$

$$\Rightarrow \boldsymbol{M}_{strip} = \int_{-1}^1 \int_0^{ns} \int_{-1}^1 \overline{\boldsymbol{N}}^T \rho\overline{\boldsymbol{N}} \det(\boldsymbol{J}) d\xi d\eta d\zeta$$

(20)

$$*\dot{\boldsymbol{u}} = \left\langle \dot{u}(\xi,\eta) \quad \dot{v}(\xi,\eta) \quad \dot{w}(\xi,\eta) \right\rangle^T$$

Note that $\hat{\dot{\boldsymbol{u}}}$ is the nodal velocity vector in Eq. (20), Using stiffness and mass matrices for each strip element $\boldsymbol{K}_{strip}, \boldsymbol{M}_{strip}$ illustrated in Eq. (17) and Eq. (20) respectively, it is possible to obtain natural frequency values by solving the eigenvalue problem shown in Eq. (21).

$$\det(\boldsymbol{K} - \omega^2 \boldsymbol{M}) = 0$$

(21)

where the matrices $\boldsymbol{K}$ and $\boldsymbol{M}$ represent stiffness and mass matrices after assembling strips and applying boundary conditions respectively.

3.4 Functionally Graded Material (FGM)

Functionally Graded Materials (FGMs) are metallurgic composite materials which have received increasing attention in structural applications in recent year. Mechanical properties of FGMs are characterized by variations in composition over the volume fraction of constituents in one or more directions that are usually made of two constitutions, ceramic and metal portions. For a sandwich shell, some layers can be FGM and the other layers can be isotropic. In an FGM layer with local coordinates in the thickness direction $\overline{\zeta}$ (see Fig. 3), this composition changes in terms of volume fraction of constituents as

$$E(\overline{\zeta}) = (E_c - E_m)V_c(\overline{\zeta}) + E_m$$

$$\nu(\overline{\zeta}) = (\nu_c - \nu_m)V_c(\overline{\zeta}) + \nu_m$$

$$\rho(\overline{\zeta}) = (\rho_c - \rho_m)V_c(\overline{\zeta}) + \rho_m$$

$$*-1 \le \overline{\zeta} \le 1$$

(22)

In Eq. (22), E_c, ν_c, ρ_c and E_m, ν_m, ρ_m denote mechanical properties of ceramic and metal respectively and V_c demonstrates volume fraction of ceramic.

By substituting $E(\overline{\zeta}), \nu(\overline{\zeta})$ and $\rho(\overline{\zeta})$ in Eqs. (19) and (20) it is possible to apply the FGM, and laminate and sandwich FGM to the shell as material properties by a uniform formulation.
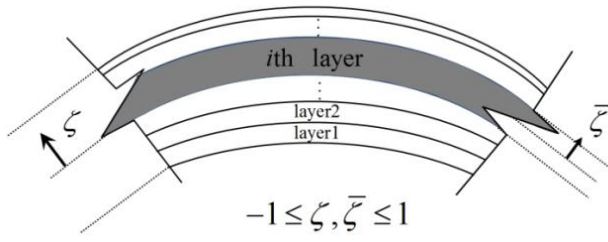
Fig. 3 Local coordinates of the entire shell (ζ) and ith layer of shell ($\bar{\zeta}$) in the thickness direction

4. Numerical results and discussion

This section exhibits several examples related to the free vibration of laminate and sandwich FGM shell panels. Most of these examples are extracted from literature to validate the accuracy of this method (Tornabene and Viola 2009, Bacciocchi *et al.* 2015, Tornabene *et al.* 2017).

4.1 FGM shell panels

The first set of examples is about the free vibration of FGM shell panels extracted from (Tornabene and Viola 2009). In the aforementioned reference two constituents have been assumed, zirconia as ceramic and aluminum as metal; similarly, two kinds of functions have also been assumed for volume fraction of ceramic ($V_c(\zeta)$), stated in Eq. (23)

$$FGM1: V_c(\bar{\zeta}) = \left(\frac{1}{2} - \frac{\bar{\zeta}}{2}\right)^r, \quad FGM2: V_c(\bar{\zeta}) = \left(\frac{1}{2} + \frac{\bar{\zeta}}{2}\right)^r \quad (23)$$

Young's modulus, Poisson's ratio, and mass density for zirconia are $E_c = 168GPa$, $v_c = 0.3$, and $\rho_c = 5700 kg/m^3$; for aluminum, they are $E_m = 70GPa$, $v_m = 0.3$, and $\rho_m = 2707 kg/m^3$.

Details regarding the geometry of the FGM shell panels with reference to Fig. 4 are demonstrated (Tornabene and Viola 2009):

1- Toro-parabolic panel: $k = 9m$, $h = 0.2m$, $R_b = 9m$, $a = 3m$, $c = -3m$, $b = 1m$, $\vartheta = 120°$

2- Parabolic panel: $k = 8m$, $h = 0.2m$, $R_b = 0$, $a = 4m$, $c = 1m$, $b = 2m$, $\vartheta = 120°$

3- Toro-circular panel: $h = 0.2m$, $R_b = -1.5m$, $R = 3m$, $\varphi_0 = 60°$, $\varphi_1 = 120°$, $\vartheta = 120°$

4- Spherical panel: $h = 0.1m$, $R_b = 0$, $R = 2m$, $\varphi_0 = 30°$, $\varphi_1 = 90°$, $\vartheta = 120°$
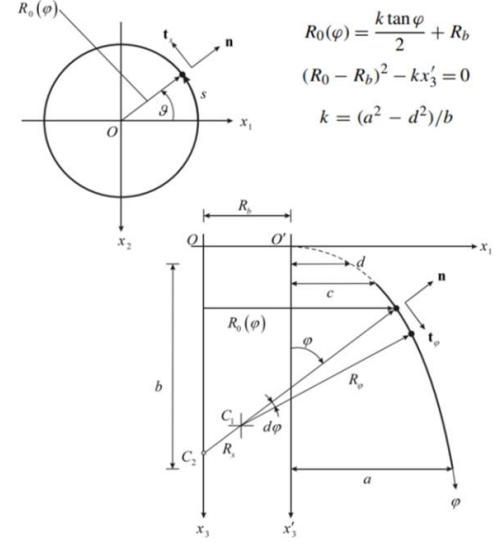

Fig. 4 Details related to the definition of geometry of the FGM shell panells (Tornabene and Viola 2009)
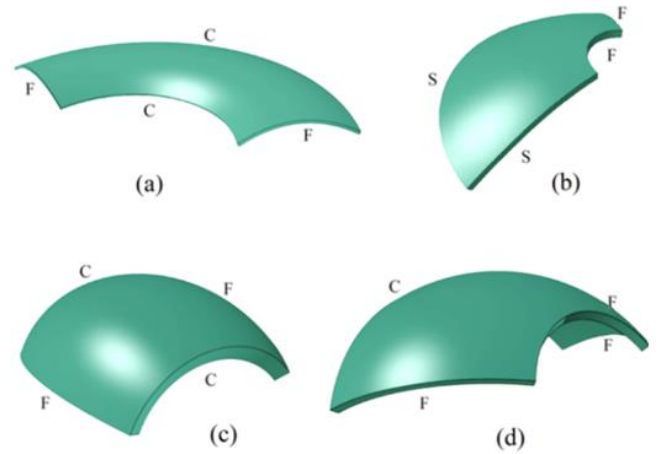
Fig. 5 Geometries and boundary conditions (Tornabene and Viola 2009): (a) Toro-parabolic panel (CFCF), (b) Parabolic panel (SSFF), (c) Toro-circular panel (CFCF) and (d) Spherical panel (CFFF)

Geometries and boundary conditions of examples concerned with the work of Tornabene and Viola (2009) are depicted in Fig. 5.

At the first step, a convergence study of results related to five natural frequency parameters of the Toro-parabolic isotropic shell (zirconia) was conducted (Fig. 5(a)). This convergence study is presented in Table 1. The frequency parameters are given for the number of strips (NST) equal to 10, 15, and 20, and the number of sections (or intervals) for each strip (NSC) equal to 8, 10, and 12. The values for NST and NSC needed for convergence depend on several parameters, like geometry of the shell, boundary conditions, and thickness variation. The results presented in Table 1 demonstrate that sufficient and accurate results are achieved when the first five modal frequencies of isotropic Toro-

Table 1 Convergence astudy of isotropic Toro-parabolic shell

ω^*	NSC=8			NSC=10			NSC=12			Tornabene and Viola (2009)
	NST=10	NST=15	NST=20	NST=10	NST=15	NST=20	NST=10	NST=15	NST=20	
1	37.540	37.487	37.465	36.836	36.780	36.757	36.782	36.726	36.703	36.620
2	38.332	38.277	38.255	37.625	37.568	37.545	37.572	37.515	37.492	37.389
3	40.993	40.965	40.953	40.351	40.322	40.309	40.329	40.300	40.286	40.191
4	46.441	46.370	46.340	45.842	45.769	45.738	45.853	45.779	45.748	45.633
5	54.185	54.045	53.997	53.618	53.477	53.428	53.649	53.507	53.458	53.268

(∗) *NSC*=Number of sections   (∗) *NST*=Number of isogeometric spline finite strips   (∗) $\omega^* = \omega k^2 \sqrt{\rho_c/(h^2 E_c)}$

Table 2 First five natural frequency parameters (ω^*) of Parabolic FGM shell panel

ω^*		r =0	r =0.6	r =1	r =5	r =20	r =50	r =100	r =∞
	FGM1- Parabolic panel		$\omega^* = \omega k^2 \sqrt{\rho_c/(h^2 E_c)}$						
1	IG-SFSM (present study)	31.424	30.217	29.902	29.969	29.891	29.680	29.565	29.424
	Tornabene and Viola (2009)	31.272	30.076	29.765	29.843	29.765	29.547	29.435	29.295
2	IG-SFSM (present study)	41.416	40.413	40.276	40.931	40.202	39.516	39.187	38.787
	Tornabene and Viola (2009)	41.183	40.250	40.131	40.798	40.024	39.320	38.983	38.576
3	IG-SFSM (present study)	64.222	62.630	62.145	61.582	61.030	60.604	60.397	60.149
	Tornabene and Viola (2009)	64.808	63.308	62.852	62.282	61.645	61.182	60.967	60.700
4	IG-SFSM (present study)	71.844	68.833	68.037	67.963	67.993	67.674	67.504	67.289
	Tornabene and Viola (2009)	72.133	69.281	68.522	68.396	68.315	67.970	67.789	67.563
5	IG-SFSM (present study)	80.929	77.751	77.048	77.807	77.451	76.681	76.288	75.800
	Tornabene and Viola (2009)	81.022	78.014	77.362	78.066	77.596	76.800	76.392	75.892
	FGM2- Parabolic panel		$\omega^* = \omega k^2 \sqrt{\rho_c/(h^2 E_c)}$						
1	IG-SFSM (present study)	31.424	30.906	30.772	30.787	30.232	29.832	29.647	29.424
	Tornabene and Viola (2009)	31.272	30.769	30.639	30.661	30.106	29.702	29.517	29.295
2	IG-SFSM (present study)	41.416	39.735	39.424	40.168	39.887	39.372	39.109	38.787
	Tornabene and Viola (2009)	41.183	39.457	39.135	39.883	39.646	39.146	38.890	38.576
3	IG-SFSM (present study)	64.222	62.952	62.571	62.082	61.223	60.682	60.437	60.149
	Tornabene and Viola (2009)	64.808	63.452	63.052	62.560	61.741	61.223	60.982	60.700
4	IG-SFSM (present study)	71.844	71.359	71.211	70.933	69.244	68.244	67.804	67.289
	Tornabene and Viola (2009)	72.133	71.541	71.359	71.044	69.433	68.481	68.056	67.563
5	IG-SFSM (present study)	80.929	79.410	79.151	79.822	78.288	77.059	76.485	75.800
	Tornabene and Viola (2009)	81.025	79.388	79.107	79.773	78.307	77.118	76.559	75.892

parabolic shells use ten strips where each strip is made of ten sections (NST = 10, NSC = 10). It is noteworthy that some modes have more complicated modal shapes and that to obtain frequencies related to these modes some more strips made of more sections may be needed.

The five first natural frequency parameters of Toro-parabolic, parabolic, Toro-circular, and spherical FGM shell panels with different boundary conditions are illustrated in Tables 3 and Table 2, Table 4 and Table 5 respectively.

Reviewing the aforementioned tables, it is clear that frequency parameters obtained by the present method (IG-SFSM) are close to the results obtained by Tornabene and Viola (2009) for similar cases using GDQ. This proximity means that the introduced finite strip method is able to obtain natural frequencies related to the free vibration of FGM shell panel's analysis with arbitrary shapes. The five first natural frequency parameters of Toro-parabolic, parabolic, Toro-circular, and spherical FGM shell panels with different boundary conditions are illustrated in Tables 3 and 5 respectively. Reviewing the aforementioned tables,

Table 4 First five natural frequency parameters (ω^*) of Toro-circular FGM shell panel

| ω^*		$r=0$	$r=0.6$	$r=1$	$r=5$	$r=20$	$r=50$	$r=100$	$r=\infty$
	FGM1- Toro-circular panel		$\omega^* = \omega R^2 \sqrt{\rho_c/(h^2 E_c)}$						
1	IG-SFSM (present study)	13.141	12.836	12.747	12.626	12.487	12.398	12.358	12.309
	Tornabene and Viola (2009)	13.111	12.781	12.687	12.565	12.444	12.363	12.325	12.281
2	IG-SFSM (present study)	13.341	13.024	12.934	12.821	12.681	12.589	12.546	12.496
	Tornabene and Viola (2009)	13.319	12.976	12.880	12.768	12.646	12.561	12.522	12.475
3	IG-SFSM (present study)	17.715	17.020	16.894	17.219	17.091	16.858	16.272	16.593
	Tornabene and Viola (2009)	17.653	16.945	16.818	17.146	17.021	16.794	16.678	16.535
4	IG-SFSM (present study)	18.179	17.458	17.329	17.678	17.549	17.305	17.181	17.028
	Tornabene and Viola (2009)	18.111	17.381	17.251	17.602	17.474	17.235	17.114	16.964
5	IG-SFSM (present study)	18.942	18.479	18.340	18.132	17.960	17.851	17.801	17.742
	Tornabene and Viola (2009)	18.944	18.451	18.304	18.098	17.947	17.846	17.800	17.744
	FGM2- Toro-circular panel		$\omega^* = \omega R^2 \sqrt{\rho_c/(h^2 E_c)}$						
1	IG-SFSM (present study)	13.141	12.916	12.848	12.713	12.519	12.412	12.364	12.309
	Tornabene and Viola (2009)	13.111	12.913	12.850	12.714	12.503	12.389	12.339	12.281
2	IG-SFSM (present study)	13.341	13.110	13.040	12.913	12.715	12.603	12.554	12.496
	Tornabene and Viola (2009)	13.319	13.114	13.052	12.924	12.708	12.589	12.536	12.475
3	IG-SFSM (present study)	17.715	17.249	17.183	17.500	17.196	16.903	16.763	16.593
	Tornabene and Viola (2009)	17.653	17.199	17.136	17.454	17.148	16.850	16.707	16.535
4	IG-SFSM (present study)	18.179	17.695	17.629	17.970	17.657	17.351	17.204	17.028
	Tornabene and Viola (2009)	18.111	17.639	17.575	17.915	17.602	17.292	17.143	16.964
5	IG-SFSM (present study)	18.942	18.717	18.577	18.372	18.062	17.896	17.825	17.742
	Tornabene and Viola (2009)	18.944	18.697	18.617	18.411	18.078	17.905	17.830	17.744
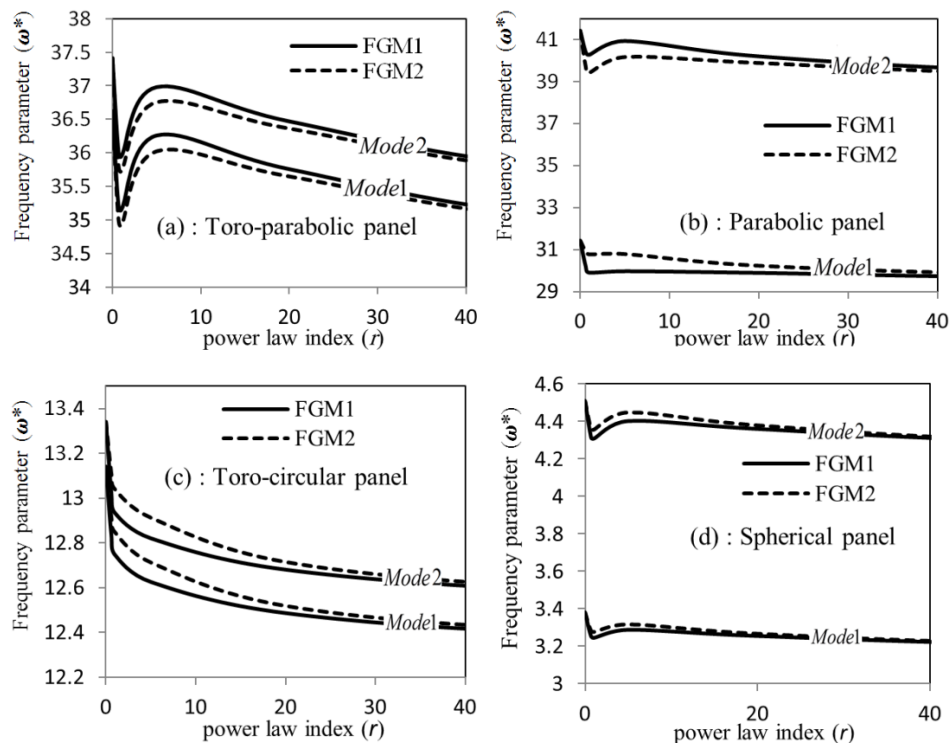
Fig. 6 Relationship between first two modal frequency parameters (ω^*) and power law index (r) related to FGM shell panels: (a) Toro-parabolic panel, (b) Parabolic panel, (c) Toro-circular panel and (d) Spherical panel

Table 5 First five natural frequency parameters (ω^*) of Spherical FGM shell panel

ω^*		$r=0$	$r=0.6$	$r=1$	$r=5$	$r=20$	$r=50$	$r=100$	$r=\infty$
		FGM1- Spherical panel		$\omega^* = \omega R^2 \sqrt{\rho_c/(h^2 E_c)}$					
1	IG-SFSM (present study)	3.380	3.266	3.244	3.287	3.254	3.212	3.191	3.166
	Tornabene and Viola (2009)	3.382	3.268	3.246	3.289	3.256	3.214	3.193	3.168
2	IG-SFSM (present study)	4.509	4.338	4.308	4.402	4.360	4.296	4.264	4.224
	Tornabene and Viola (2009)	4.506	4.334	4.305	4.399	4.358	4.293	4.261	4.221
3	IG-SFSM (present study)	7.017	6.774	6.729	6.830	6.762	6.672	6.627	6.573
	Tornabene and Viola (2009)	7.013	6.769	6.725	6.826	6.758	6.668	6.624	6.569
4	IG-SFSM (present study)	8.315	7.984	7.930	8.134	8.061	7.932	7.868	7.788
	Tornabene and Viola (2009)	8.321	7.977	7.923	8.128	8.055	7.926	7.862	7.782
5	IG-SFSM (present study)	11.252	10.914	10.839	10.888	10.778	10.663	10.607	10.540
	Tornabene and Viola (2009)	11.243	10.904	10.830	10.880	10.770	10.655	10.599	10.531
		FGM2- Spherical panel		$\omega^* = \omega R^2 \sqrt{\rho_c/(h^2 E_c)}$					
1	IG-SFSM (present study)	3.380	3.291	3.275	3.316	3.266	3.216	3.194	3.166
	Tornabene and Viola (2009)	3.382	3.292	3.277	3.318	3.268	3.219	3.196	3.168
2	IG-SFSM (present study)	4.509	4.375	4.356	4.448	4.379	4.301	4.268	4.224
	Tornabene and Viola (2009)	4.506	4.372	4.353	4.446	4.377	4.302	4.265	4.221
3	IG-SFSM (present study)	7.017	6.825	6.793	6.890	6.786	6.678	6.633	6.573
	Tornabene and Viola (2009)	7.013	6.820	6.788	6.886	6.782	6.679	6.629	6.569
4	IG-SFSM (present study)	8.315	8.057	8.022	8.227	8.100	7.943	7.877	7.788
	Tornabene and Viola (2009)	8.321	8.050	8.015	8.221	8.093	7.944	7.870	7.782
5	IG-SFSM (present study)	11.252	10.996	10.942	10.991	10.821	10.677	10.617	10.540
	Tornabene and Viola (2009)	11.243	10.986	10.933	10.983	10.812	10.674	10.609	10.531

it is clear that frequency parameters obtained by the present method (IG-SFSM) are close to the results obtained by Tornabene and Viola (2009) for similar cases using GDQ.

This proximity means that the introduced finite strip method is able to obtain natural frequencies related to the free- vibration of FGM shell panel's analysis with arbitrary shapes.

As can be observed in graphs depicted in Fig. 6, the relationship between the first two modal frequency parameters (ω^*) and the power law index (r) is plotted between r equal to 0 and 40 as low and high level values of the power-law index.

With reference to Eq. (23), it is apparent that r equal to 0 denotes the full ceramic shell: higher values for this parameter represent the shell with characteristics approximately close to the full metal. By considering the graphs depicted in Fig. 6 it can be seen that there are some notable points. For all of the cases except the Toro-circular panel in the intermediate range in the vicinity of r equal to 1, modal frequency parameters do not have uniform changes. In this range, the influence of the chosen ceramic's volume fraction function (i.e., FGM1 or FGM2) on modal frequency parameters is varies more significantly from each other, whereas at very high or low levels for values of r these differences are insignificant. As can be seen in Figs. 6(a)-6(c), the first and second modal frequencies of the Toro-parabolic and Toro-circular panels are close to each other for all values of the power-law index (r) and the choice of ceramic's volume fraction. However, as demonstrated in Figs. 6(b)-6(d) for cases with parabolic and spherical panels.
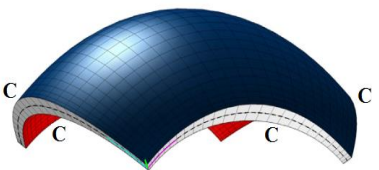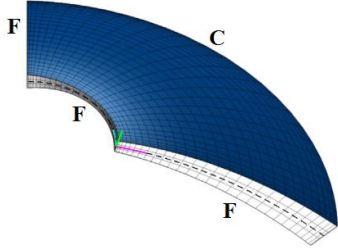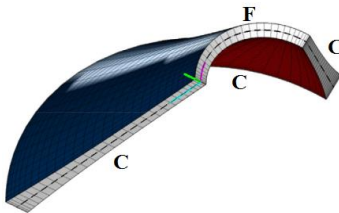
4.2 Laminated shell panels with variable thickness

The second set of examples is related to shell panels with two important characteristics. All the cases have variable thickness and are made of laminated materials (Bacciocchi *et al.* 2015). Three types of materials are used as constituents in these laminations. Mechanical properties of these constituent materials are illustrated in Table 6.

To define the geometry of the shells in this set of examples, we considered an arbitrary curved surface defined in global and local curvilinear coordinates as depicted in Fig. 7 Definition of geometry using this manner allowed us to introduce the geometrical characteristics of this set of examples. By means of this method, three geometric types of shell panels with their variation of thickness can be defined as demonstrated in Table 7. These geometrical characteristics and variation of thickness representations are defined based on Eq. (24) and Fig. 7.

$$\vec{r}(\alpha_1, \alpha_2) = x(\alpha_1, \alpha_2)\boldsymbol{e}_x + y(\alpha_1, \alpha_2)\boldsymbol{e}_y + z(\alpha_1, \alpha_2)\boldsymbol{e}_z$$
$$h(\alpha_1, \alpha_2) = h_0 f(\alpha_1, \alpha_2) \tag{24}$$
$$\alpha_1 = [\alpha_1^0, \alpha_1^1] \quad , \quad \alpha_2 = [\alpha_2^0, \alpha_2^1]$$

Table 6 Mechanical properties of material constituents related to second set of examples (Bacciocchi *et al.* 2015)

	$E(GPa)$	ν	$\rho(kg/m^3)$
Aluminum	70	0.3	2707
Zirconia	168	0.3	5800
Steel	210	0.3	7800

Table 7 Geometrical characteristics of laminated shell panels (Bacciocchi *et al.* 2015)

Translational panel (CCCC)	Panel of revolution (FCFF)	Conical panel (FCCC)

$x = R_0^{\alpha_1}(\alpha_1) - S_0^{\alpha_2}(\alpha_2)\sin\alpha_1$

$y = -R_0^{\alpha_2}(\alpha_2)$

$z = S_0^{\alpha_1}(\alpha_1) + S_0^{\alpha_2}(\alpha_2)\cos\alpha_1$

$f = 1 - \dfrac{1}{4}\sin\left(2\dfrac{\alpha_1 - \alpha_1^0}{\alpha_1^1 - \alpha_1^0}\pi + \dfrac{\pi}{2}\right) +$

$\quad - \dfrac{1}{4}\sin\left(2\dfrac{\alpha_2 - \alpha_2^0}{\alpha_2^1 - \alpha_2^0}\pi + \dfrac{\pi}{2}\right)$

$\{\alpha_1^0, \alpha_2^0, \alpha_1^1, \alpha_2^1\} = \{\frac{-\pi}{4}, \frac{-\pi}{4}, \frac{\pi}{4}, \frac{\pi}{4}\}$

$a = 1m, h_0 = 0.1m$

$x = a\sinh(\tan\alpha_1)\cos\alpha_2$

$y = -a\sinh(\tan\alpha_1)\sin\alpha_2$

$z = a(\cosh(\text{arcsinh}(\tan\alpha_1)) - 1)$

$f = 1 + \dfrac{3}{2}\left(\dfrac{\alpha_1 - \alpha_1^0}{\alpha_1^1 - \alpha_1^0}\right) - \dfrac{1}{2}\sin\left(\dfrac{\alpha_2 - \alpha_2^0}{\alpha_2^1 - \alpha_2^0}\right)$

$\{\alpha_1^0, \alpha_2^0, \alpha_1^1, \alpha_2^1\} = \{\frac{\pi}{12}, 0, \frac{\pi}{4}, \frac{\pi}{2}\}$

$a = 1m, h_0 = 0.045m$

$x = a\cos\alpha_1 +$

$\quad + \alpha_2\sin\theta\sin(\arctan(-\cot\alpha_1))$

$y = -\alpha_2\cos\theta$

$z = a\sin\alpha_1 +$

$\quad + \alpha_2\sin\theta\cos(\arctan(-\cot\alpha_1))$

$f = 1 + \left(\dfrac{\alpha_2 - \alpha_2^0}{\alpha_2^1 - \alpha_2^0}\right)^3$

$\{\alpha_1^0, \alpha_2^0, \alpha_1^1, \alpha_2^1\} = \{0, 0, \frac{2\pi}{3}, L_y\}$

$a = 0.5m, h_0 = 0.1m, \theta = \pi/6, L_y = 2m$

$R_0^{\alpha_1} = a\sin\alpha_1 \quad R_0^{\alpha_2} = a\sin\alpha_2 \quad S_0^{\alpha_1} = a(1 - \cos\alpha_1) \quad S_0^{\alpha_2} = a(1 - \cos\alpha_2)$

Table 8 First ten natural frequencies of translational panel, panel of revolution, and conical panel

ω^*	Translational panel (CCCC)		Panel of revolution (FCFF)		Conical panel (FCCC)	
	present	Bacciocchi *et al.* (2015)	present	Bacciocchi *et al.* (2015)	present	Bacciocchi *et al.* (2015)
1	11.731	11.716	9.892	9.888	1.5632	1.5622
2	11.810	11.800	10.851	10.839	1.8204	1.8195
3	12.778	12.758	21.539	21.522	2.3325	2.3314
4	15.911	15.892	25.347	25.338	2.3976	2.3965
5	17.525	17.506	26.112	26.075	2.5345	2.5332
6	19.446	19.426	40.932	40.940	3.0861	3.0844
7	20.011	19.994	41.530	41.503	3.1297	3.1274
8	20.261	20.237	47.083	47.075	3.2448	3.2428
9	22.008	21.990	47.608	47.565	3.3262	3.3248
10	22.228	22.205	52.716	52.659	3.7657	3.7637

$\omega^* = \omega a^2 \sqrt{\dfrac{\rho_{Al}}{E_{Al}h_0^2}}$

Lamination scheme : (Al/Zi)
$h_{0,1}$=0.05m $h_{0,2}$=0.05 m

Lamination scheme : (Al/Zi/Al)
$h_{0,1}$=0.015m, $h_{0,2}$=0.015 m $h_{0,3}$=0.015 m

Lamination scheme : (Al/St)
$h_{0,1}$=0.05 m $h_{0,2}$=0.05 m

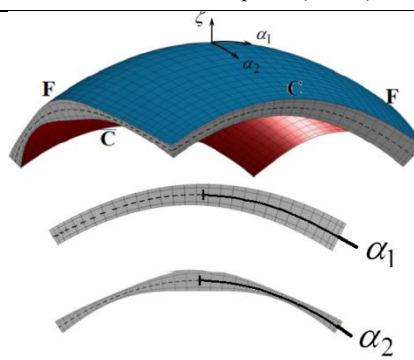Table 9 Geometrical characteristics of sandwich FGM translational shell panel (Tornabene *et al*. 2017)

Translational shell panel (CFCF)	Geometrical characteristics
	$x = \dfrac{k \tan \alpha_1}{2} - \dfrac{k \tan^2 \alpha_2}{4} \sin \alpha_1$, $y = -\dfrac{k \tan \alpha_2}{2}$, $\alpha_{1,2} \in [\alpha_{1,2}^0, \alpha_{1,2}^1]$ $z = \dfrac{k \tan^2 \alpha_1}{4} + \dfrac{k \tan^2 \alpha_2}{4} \cos \alpha_1$, $k = (a^2 - d^2)/b$, $a = 3m, b = 1m$ $c = -3m, d = 0$, $\alpha_1^0 = \alpha_2^0 = -0.588003$, $\alpha_1^1 = \alpha_2^1 = 0.588003$ $h(\alpha_1, \alpha_2) = h_0 \left(1 + \dfrac{3}{4} \left(\dfrac{\alpha_1 - \alpha_1^0}{\alpha_1^1 - \alpha_1^0} \right)^2 + \dfrac{1}{2} \sin \left(\pi \left(3 \left(\dfrac{\alpha_2 - \alpha_2^0}{\alpha_2^1 - \alpha_2^0} \right) + 1 \right) \right) \right)$ $h_{0,1} = h_{0,3} = 0.05m$, $h_{0,2} = 0.2m$, $h_0 = h_{0,1} + h_{0,2} + h_{0,3} = 0.3m$

Table 10 Mechanical properties of material constituents related to third example (Tornabene *et al*. 2017)

	$E(GPa)$	ν	$\rho(kg/m^3)$
Stainless steel	207.7877	0.317756	8166
Silicon nitride $Si_3 N_4$	322.2715	0.24	2370

All three laminated shell panels represented in Table 7 based on Eq. (24) and Fig. 7 were analyzed by IG-SFSM. The results so obtained were compared with results for similar cases presented by Bacciocchi *et al*. (2015) based on the GDQ method. This comparison is demonstrated in Table 8: it shows the closeness of two kinds of results for each case of study. This comparison presents proof of the accuracy of the present method in analysis of laminated shell panels with variable thickness incorporating arbitrary shapes and various boundary conditions (Bacciocchi *et al*. 2015).

4.3 Sandwich FGM shell panel of variable thickness

The third example is related to free vibration analysis and natural frequencies of a doubly curved translational sandwich FGM shell panel (Tornabene *et al*. 2017). Geometrical characteristics and variation of the thickness representation of this shell and the applied boundary condition are depicted in Table 9. These characteristics are presented based on the description in Fig. 7. This example incorporates a doubly curved translational shell made of three different layers. The first layer (down layer) is made of stainless steel SUS304, the middle layer is made of FGM1 that is shown in Eq. (23), and third layer (top layer) is made of Silicon nitride Si_3N_4. Mechanical properties of the material constituents employed in FGM related to this example are demonstrated in Table 10.

The first eight natural frequencies of a doubly curved translational sandwich FGM shell panel introduced in Tables 9 and 10 have been analyzed using IG-SFSM: the

results obtained were compared with those related to same case, have been achieved by Tornabene *et al*. (2017) using local generalized differential quadrature (LGDQ). This comparison is demonstrated in Table 11: it shows the suitable accuracy of the introduced IG-SFSM. Investigation of Table 11 shows that for each mode of natural frequencies, there is a special relationship between the modal frequency and the power-law index (*r*).
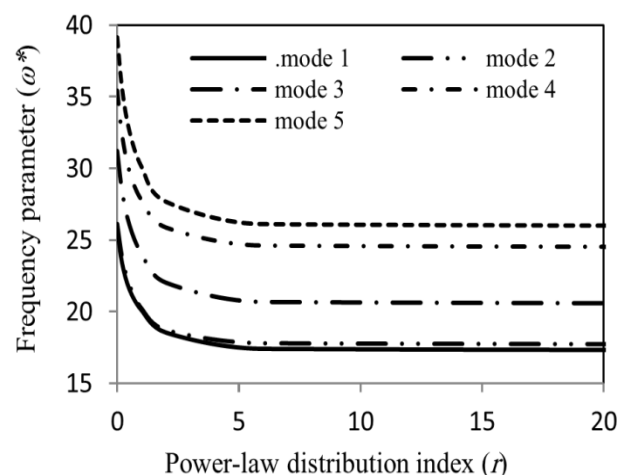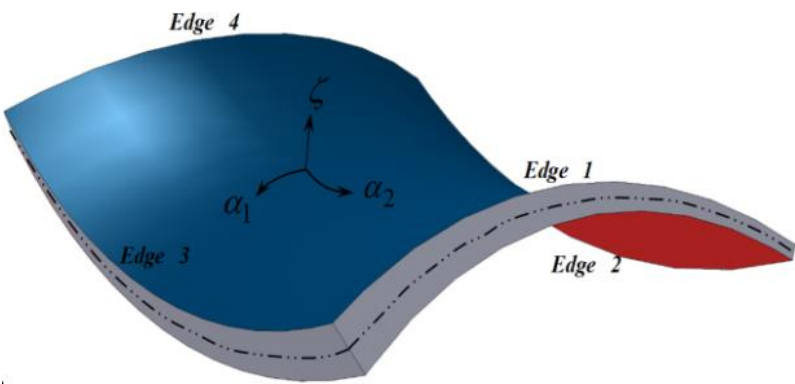

Fig. 8 Relationship between first five modal frequency parameter (ω^*) and power law index (*r*) related to doubly curved sandwich FGM shell panel

Table 11 First ten natural frequency parameters (ω^*) of doubly curved sandwich FGM shell panel

ω^*	Doubly curved Sandwich FGM shell panel	$r = 0$	$r = 0.2$	$r = 0.5$	$r = 1$	$r = 2$	$r = 6$	$r = 128$	$r = \infty$
					$\omega^* = \omega k^2 \sqrt{\rho_c/(h^2 E_c)}$				
1	IG-SFSM (present study)	28.548	25.639	23.375	21.557	20.096	18.545	17.406	17.341
	Tornabene *et al.* (2017)	28.345	25.457	23.204	21.406	19.950	18.509	17.374	17.307
2	IG-SFSM (present study)	29.001	26.123	23.808	21.879	20.225	18.716	17.795	17.739
	Tornabene *et al.* (2017)	28.941	26.069	23.759	21.835	20.182	18.723	17.662	17.607
3	IG-SFSM (present study)	34.696	31.211	28.402	26.058	24.048	22.027	20.680	20.603
	Tornabene *et al.* (2017)	34.670	31.188	28.378	26.036	24.026	22.005	20.661	20.582
4	IG-SFSM (present study)	39.432	35.426	32.301	29.800	27.780	25.876	24.613	24.537
	Tornabene *et al.* (2017)	39.317	35.323	32.204	29.711	27.692	25.793	24.531	24.456
5	IG-SFSM (present study)	43.659	39.142	35.550	32.595	30.108	27.674	26.110	26.021
	Tornabene *et al.* (2017)	43.643	39.128	35.534	32.582	30.095	27.661	26.098	26.010
6	IG-SFSM (present study)	48.756	43.611	39.471	36.024	33.078	30.155	28.298	28.196
	Tornabene *et al.* (2017)	48.742	43.598	39.460	36.016	33.068	30.146	28.290	28.188
7	IG-SFSM (present study)	56.278	50.496	45.959	42.304	39.323	36.504	34.684	34.578
	Tornabene *et al.* (2017)	56.219	50.443	45.908	42.260	39.279	36.467	34.649	34.543
8	IG-SFSM (present study)	61.181	54.768	49.741	45.696	42.421	39.356	37.402	37.289
	Tornabene *et al.* (2017)	61.041	54.643	49.623	45.594	42.320	39.262	37.311	37.197

Table 12 Geometrical characteristics of laminated-sandwich FGM hyperbolic paraboloid shell panel

hyperbolic paraboloid shell panel	Geometrical characteristics
Lamination scheme : (Al/St/FGM2/Si/Zi)	$x = \dfrac{k \tan \alpha_1}{2} + \dfrac{k \tan^2 \alpha_2}{4} \sin \alpha_1$ $y = \dfrac{k \tan \alpha_2}{2}$, $\alpha_{1,2} \in [\alpha_{1,2}^0, \alpha_{1,2}^1]$ $z = -\dfrac{k \tan^2 \alpha_1}{4} + \dfrac{k \tan^2 \alpha_2}{4} \cos \alpha_1$ $k = (a^2 - d^2)/b, a = 3m, b = 1m$ $c = -3m, d = 0$, $\alpha_1^0 = \alpha_2^0 = -0.59$ $\alpha_1^1 = \alpha_2^1 = 0.59$ $h(\alpha_1, \alpha_2) = h_0 \left(1 + \dfrac{3}{4} \left(\dfrac{\alpha_1 - \alpha_1^0}{\alpha_1^1 - \alpha_1^0} \right)^2 + \dfrac{2}{3} \left(\dfrac{\alpha_2 - \alpha_2^0}{\alpha_2^1 - \alpha_2^0} \right)^4 \right)$ $h_{0,1} = h_{0,2} = h_{0,4} = h_{0,5} = 0.025m$, $h_{0,3} = 0.3m$ $h_0 = \sum_{i=1}^{5} h_{0,i} = 0.4m$

Fig. 8 shows this relationship for the first five modal frequencies. Investigation of Fig. 8 shows that the manner of change of all modal frequency parameters is the same, but increase in the number of modes results in increase in the maximum and minimum modal frequencies. It is notable that for each mode of natural frequency, increasing the power-law index (*r*) to more than 5 results in the same frequency which converges to the special value. This manner is different from that demonstrated in Fig. 6, related as that is to the first set of examples.

4.4 Laminated-sandwich FGM shell panel with variable thickness

The last numerical example is about free vibration of a laminated-sandwich FGM shell panel with variable thickness. The geometry of the aforementioned shell panel is hyperbolic paraboloid. Natural frequencies of the aforementioned structures have been calculated using IG-SFSM for different boundary conditions and FGM representations. Table 12 demonstrates the geometrical characteristics of laminated and sandwich FGM hyperbolic paraboloid shell panels. Notably, the appellation of different

Table 13 Natural frequency parameters of hyperbolic paraboloid shell panel for different boundary conditions

ω^*	SSSS	CCCC	SCCS	CSSC	SFFS	FSSF	CFFC	FCCF	FSCF	SFFC
					r =1					
1	246.41	281.62	253.26	276.59	171.97	149.97	220.37	166.80	162.42	188.51
2	260.63	310.91	266.96	282.78	201.40	162.37	228.05	187.89	174.10	203.47
3	266.45	322.82	306.86	304.81	206.80	169.19	235.27	197.32	183.14	220.94
4	300.85	386.03	337.44	356.22	211.20	181.94	250.02	219.44	203.31	236.55
5	379.08	471.18	388.30	401.66	231.31	215.46	280.22	232.21	217.01	247.83
6	386.15	473.49	453.60	465.30	260.10	249.76	321.81	289.03	268.39	288.80
					r =3					
1	217.66	246.76	223.94	241.95	152.33	133.01	193.26	146.34	142.37	166.34
2	227.12	275.48	233.17	249.76	178.02	142.05	200.24	165.23	154.36	178.44
3	234.83	285.99	271.56	269.92	181.13	150.16	208.94	175.58	161.25	194.20
4	267.45	343.27	300.03	316.66	184.45	159.68	220.71	192.99	180.68	208.71
5	337.56	418.91	345.73	357.32	203.56	188.92	248.80	206.49	190.44	219.44
6	343.45	420.92	403.39	413.68	231.44	221.81	286.09	256.86	238.42	257.07
					r =5					
1	209.46	236.79	215.73	231.86	146.81	128.16	185.43	140.53	136.49	160.17
2	217.58	265.52	223.75	240.16	171.31	136.05	192.22	158.86	148.75	171.53
3	225.91	275.44	261.70	259.98	174.13	144.85	201.48	169.52	155.06	186.54
4	258.01	331.16	289.64	305.28	177.11	153.26	212.35	185.39	174.45	200.98
5	325.79	404.03	333.77	344.55	195.99	181.10	239.90	199.34	182.68	211.28
6	331.31	406.09	389.27	399.02	223.74	213.50	276.05	247.57	229.66	248.25

$$\omega^* = \omega k^2 \sqrt{\rho_{Si}/(h_0^2 E_{Si})}$$

boundary conditions is based on Edge 1, Edge 2, Edge 3, and Edge 4, as shown in Table 12. For example, FCSF represents the special boundary condition wherein Edge 1 is the free edge (i.e. all DOFs are free); Edge 2 is completely clamped, i.e. all edges are restrained; Edge 3 is completely simple, i.e. all translational DOFs are restrained and all rotational DOFs are free; and Edge 4 is another free edge. This shell panel is made of five layers. The first and second layers are made of aluminum and steel respectively. The third and fourth layers are made of silicon and zirconia respectively. The middle layer is made of functionally graded material such that the governing function in this layer is related to FGM2, as illustrated in Eq. (23). This layer is made of two constituent materials, ceramic (silicon) and metal (steel). The mechanical properties of aluminum, steel and zirconia are demonstrated in Table 6; these characteristics for silicon are presented in Table 10. The natural frequency parameters of free vibration have been achieved for the aforementioned shell panel: relevant results are shown in Table 13, demonstrating the effect of boundary condition on the natural frequencies of free vibration.

5. Conclusions

In the present paper, an improved version of FSM, named IG-SFSM, is introduced. The method is able to model shell structures with different complicated geometries and boundary conditions. By employing the FEM and IGA in the transverse and longitudinal directions, respectively, and enjoying the benefits of the methods, multipurpose targets are achieved for analysis of the sandwich FGM shells. To show the accuracy of the method, different examples related to the free vibration analysis of shell structures with different geometries, boundary conditions, and material properties are considered. Most of them are available in the existing literature, which employed the other numerical methods: these are used for validating of the results achieved by IG-SFSM. Free vibration analysis and obtained natural frequencies, show that it is possible to analyze the shell structures with the aforementioned mechanical and geometrical properties by means of IG-SFSM. Also, the corresponding results show that the method is an efficient tool in comparison to the other methods, such as FEM and IGA. By using IG-SFSM, the suitable continuity of IGA is provided in longitudinal direction of the strips and its shortcomings are reduced in the transversal direction by employing FEM. The introduced finite strip method provides a situation which satisfies all of the boundary conditions without any difficulties encountered with previous versions of FSM and IGA for analysis of shell structures. Results obtained by means of IG-SFSM show that there are no restrictions on use of the proposed method for free vibration analysis of sandwich functionally graded shells with the field of thickness changes.

References

Abdelaziz, H.H., Meziane, M.A.A., Bousahla, A.A., Tounsi, A., Mahmoud, S.R. and Alwabli, A.S. (2017), "An efficient hyperbolic shear deformation theory for bending, buckling and free vibration of FGM sandwich plates with various boundary conditions", *Steel. Compos. Struct.*, **25**(6), 693-704. https://doi.org/10.12989/scs.2017.25.6.693.

Au, F.T.K. and Cheung, Y.K. (1996), "Free vibration and stability analysis of shells by the isoparametric spline finite strip method", *Thin-Wall. Struct.*, **24**(1), 53-82. https://doi.org/10.1016/0263-8231(95)00040-2.

Bacciocchi, M., Eisenberger, M., Fantuzzi, N., Tornabene, F. and Viola, E. (2015), "Vibration analysis of variable thickness plates and shells by the Generalized Differential Quadrature method", *Compos. Struct.*, **156**, 218-237. https://doi.org/10.1016/j.compstruct.2015.12.004.

Belabed, Z., Bousahla, A.A., Houari, M.S.A., Tounsi, A. and Mahmoud, S.R. (2018), "A new 3-unknown hyperbolic shear deformation theory for vibration of functionally graded sandwich plate", *Earthq. Struct.*, **14**(2), 103-115. https://doi.org/10.12989/eas.2018.14.2.103.

Benson, P.R. and Hinton, E. (1976), "A thick finite strip solution for static, free vibration and stability problems", *Int. J. Numer. Method. Eng.*, **10**(3), 665-678. https://doi.org/10.1002/nme.1620100314.

Bounouara, F., Benrahou, K.H., Belkorissat, I. and Tounsi, A. (2016), "A nonlocal zeroth-order shear deformation theory for free vibration of functionally graded nanoscale plates resting on elastic foundation", *Steel. Compos. Struct.*, **20**(2), 227-249. https://doi.org/10.12989/scs.2016.20.2.227.

Bourada, F., Bousahla, A.A., Bourada, M., Azzaz, A., Zinata, A., and Tounsi, A. (2019), "Dynamic investigation of porous functionally graded beam using a sinusoidal shear", *Wind. Struct.*, **28**(1), 19-30. https://doi.org/10.12989/was.2019.28.1.019.

Bourada, M., Kaci, A., Houari, M.S.A. and Tounsi, A. (2015), "A new simple shear and normal deformations theory for functionally graded beams", *Steel. Compos. Struct.*, **18**(2), 409-423. https://doi.org/10.12989/scs.2015.18.2.409.

Chieslar, J.D. and Ghali, A. (1987), "Solid to shell element geometric transformation", *Comput. Struct.*, **25**(3), 451-455. https://doi.org/10.1016/0045-7949(87)90136-2.

Darilmaz, K. (2017), "Static and free vibration behaviour of orthotropic elliptic paraboloid shells", *Steel Compos. Struct.*, **23**(6), 737-746. https://doi.org/10.12989/scs.2017.23.6.737.

Dawe, D.J. and Wang, S. (1992), "Vibration of shear-deformable beams using a spline function approach", *Int. J. Numer. Method. Eng.*, **33**(4), 819-844. https://doi.org/10.1002/nme.1620330410.

Dvorkin, E.N. and Bathe, K. (1984), "A continuum mechanics based four-node shell element for general non-linear analysis", *Eng. Comput.*, **1**(1), 77-88. https://doi.org/10.1108/eb023562.

Eccher, G., Rasmussen, K.J.R. and Zandonini, R. (2008), "Isoparametric spline finite strip method for the bending of perforated plates", *Int. J. Numer., Method. Eng.*, **74**(9), 1448-1472 https://doi.org/10.1002/nme.2220.

El-Haina, F., Bakora, A., Bousahla, A. A., Tounsi, A., and Mahmoud, S. R. (2017), "A simple analytical approach for thermal buckling of thick functionally graded sandwich plates", *Struct. Eng. Mech.*, **63**(5), 585-595. https://doi.org/10.12989/sem.2017.63.5.585.

Fan, S.C. and Cheung, Y.K. (1983), "Analysis of shallow shells by spline finite strip method", *Eng. Struct.*, **5**(4), 255–263. https://doi.org/10.1016/0141-0296(83)90004-4.

Fan, S.C. and Luah, M.H. (1990), "New spline finite element for analysis of shells of revolution", *J. Eng. Mech.*, **116**(3), 709-726. https://doi.org/10.1061/(ASCE)0733-9399(1990)116:3(709).

Foroughi, H. and Azhari, M. (2014), "Mechanical buckling and free vibration of thick functionally graded plates resting on elastic foundation using the higher order B-spline finite strip method", *Meccanica,* **49**(4), 981–993. http-://doi.org/10.1007/s11012-013-9844-2.

Hu, X. (1997), "Free vibration analysis of symmetrical cylindrical honeycomb panels by using the finite strip method", *J. Vib. Control,* **3**(1), 19-32. https://doi.org/10.1177%2F107754639700300103 /.

Jabareen, M. and Mtanes, E. (2018), "A solid-shell Cosserat point element for the analysis of geometrically linear and nonlinear laminated composite structures", *Finite Elem. Anal. Des.*, **142**, 61-80. https://doi.org/10.1016/j.finel.2017.12.006.

Javed, S., Viswanathan, K.K. and Aziz, Z.A. (2016), "Free vibration analysis of composite cylindrical shells with non-uniform thickness walls", *Steel Compos. Struct.*, **20**(5), 1087-1102. http://dx.doi.org/10.12989/scs.2016.20.5.1087.

Karami, B., Janghorban, M. and Tounsi, A. (2018), "Nonlocal strain gradient 3D elasticity theory for anisotropic spherical nanoparticles", *Steel. Compos. Struct.*, **27**(2), 201-216. https://doi.org/10.12989/scs.2018.27.2.201.

Kim, H.J., Seo, Y.D., and Youn, S.K. (2010), "Isogeometric analysis with trimming technique for problems of arbitrary complex topology", *Comput. Method. Appl. M.*, **199**(45-48), 2796-2812. https://doi.org/10.1016/j.cma.2010.04.015.

Kwon, Y.B. and Hancock, G.J. (1991), "A nonlinear elastic spline finite strip analysis for thin-walled sections", *Thin-Wall. Struct.*, **12**(4), 295-319. https://doi.org/10.1016/0263-8231(91)90031-D.

Li, W.Y., Tham, L.G., Cheung, Y.K. and Fan, S.C. (1990), "Free vibration analysis of doubly curved shells by spline finite strip method", *J. Sound Vib.*, **140**(1), 39-53. https://doi.org/10.1016/0022-460X(90)90905-F.

Menasria, A., Bouhadra, A., Tounsi, A., Bousahla, A.A. and Mahmoud, S.R. (2017), "A new and simple HSDT for thermal stability analysis of FG sandwich plates", *Steel. Compos. Struct.*, **25**(2), 157-175. https://doi.org/10.12989/scs.2017.25.2.157.

Naghsh, A., Saadatpour, M.M. and Azhari, M. (2015), "Free vibration analysis of stringer stiffened general shells of revolution using a meridional finite strip method", *Thin-Wall. Struct.*, **94**, 651-662. https://doi.org/10.1016/j.tws.2015.05.015.

Nguyen, V.P., Anitescu, C., Bordas, S.P., and Rabczuk, T. (2015), "Isogeometric analysis: an overview and computer implementation aspects", *Math. Comput. Simulat.*, **117**, 89-116. https://doi.org/10.1016/j.matcom.2015.05.008.

Pang, F., Li, H., Wang, X., Miao, X. and Li, S. (2018), "A semi analytical method for the free vibration of doubly-curved shells of revolution", *Comput. Math. with Appl.*, **75**(9), 3249-3268. https://doi.org/10.1016/j.camwa.2018.01.045.

Piegl, L. and Tiller, W. (1997), "*The NURBS Book*", Springer-Verlag Berlin, Heidelberg, Baden-Württemberg, Germany.

Rezaiee-Pajand, M. and Arabi, E. (2016), "A curved triangular element for nonlinear analysis of laminated shells", *Compos. Struct.*, **153**, 538-548. https://doi.org/10.1016/j.compstruct.2016.06.052.

Rypl, D., and Patzák, B. (2012), "From the finite element analysis to the isogeometric analysis in an object oriented computing environment", *Adv. Eng. Softw.*, **44**(1), 116-125. https://doi.org/10.1016/j.advengsoft.2011.05.032.

Shahmohamadi, M.A. and Kabir, M.Z. (2017), "Effects of shear deformation on mechanical and thermo-mechanical nonlinear stability of FGM shallow spherical shells subjected to uniform external pressure", *Sci. Iran.*, **24**(2), 584-596. https://dx.doi.org/10.24200/sci.2017.2420.

Sheikh, A.H. (2004), "An efficient technique to include shear deformation in spline finite strip analysis of composite plates", *Int. J. Comput. Methods*, **1**(3), 491-505. https://doi.org/10.1142/S0219876204000241.

Tornabene, F., Fantuzzi, N., Bacciocchi, M., Viola, E. and Reddy, J. (2017), "A Numerical Investigation on the Natural Frequencies of FGM Sandwich Shells with Variable Thickness by the Local Generalized Differential Quadrature Method", *Appl. Sci.*, **7**(2), 131. https://doi.org/10.3390/app7020131.

Tornabene, F. and Viola, E. (2009), "Free vibration analysis of functionally graded panels and shells of revolution", *Meccanica*, **44**(3), 255–281. https://doi.org/10.1007/s11012-008-9167-x.

Uhm, T.-K. and Youn, S.-K. (2009), "T-spline finite element method for the analysis of shell structures", *Int. J. Numer. Method. Eng.*, **80**(4), 507-536. https://doi.org/10.1002/nme.2648.

Van Erp, G.M. and Menken, C.M. (1990), "Spline finite-strip method in the buckling analyses of thin-walled structures", *Commun. Appl. Numer. Methods*, **6**(6), 477-484. https://doi.org/10.1002/cnm.1630060608.

Van Erp, G.M., Yuen, S.W. and Swannell, P. (1994), "A new type of B3-spline interpolation", *Commun. Appl. Numer. Methods.*, **10**(12), 1013-1020. https://doi.org/10.1002/cnm.1640101207.

Ventsel, E. and Krauthammer, T. (2001), "*Thin Plates and Shells: Theory: Analysis, and Applications*", Marcel Dekker, New York City, New York, USA.

Vu-Bac, N., Duong, T.X., Lahmer, T., Zhuang, X., Sauer, R.A., Park, H.S. and Rabczuk, T. (2018), "A NURBS-based inverse analysis for reconstruction of nonlinear deformations of thin shell structures", *Comput. Method. Appl. M.*, **331**, 427-455. https://doi.org/10.1016/j.cma.2017.09.034.

Wang, S. and Dawe, D.J. (1999), "Buckling of composite shell structures using the spline finite strip method", *Compos. Part B Eng.*, **30**(4), 351-364. https://doi.org/10.1016/S1359-8368(99)00005-0.

Younsi, A., Tounsi, A., Zaoui, F.Z., Bousahla, A.A. and Mahmoud, S.R. (2018), "Novel quasi-3D and 2D shear deformation theories for bending and free vibration analysis of FGM plates", *Geomech. Eng.*, **14**(6), 519-532. https://doi.org/10.12989/gae.2018.14.6.519.

Zemri, A., Houari, M.S.A., Bousahla, A.A. and Tounsi, A. (2015), "A mechanical response of functionally graded nanoscale beam: an assessment of a refined nonlocal shear deformation theory beam theory", *Struct. Eng. Mech.*, **54**(4), 693-710. https://doi.org/10.12989/sem.2015.54.4.693.

Zine, A., Tounsi, A., Draiche, K., Sekkal, M. and Mahmoud, S.R. (2018), "A novel higher-order shear deformation theory for bending and free vibration analysis of isotropic and multilayered plates and shells", *Steel Compos. Struct.*, **26**(2), 125-137. https://doi.org/10.12989/scs.2018.26.2.125.

CC